Localization transition, spectrum structure, and winding numbers for one-dimensional non-Hermitian quasicrystals

Yanxia Liu,[1] Qi Zhou,[2,*] and Shu Chen[1,3,4,†]

[1]*Beijing National Laboratory for Condensed Matter Physics, Institute of Physics, Chinese Academy of Sciences, Beijing 100190, China*
[2]*Chern Institute of Mathematics and LPMC, Nankai University, Tianjin 300071, China*
[3]*School of Physical Sciences, University of Chinese Academy of Sciences, Beijing 100049, China*
[4]*Yangtze River Delta Physics Research Center, Liyang, Jiangsu 213300, China*

By analyzing the Lyapunov exponent (LE), we develop a rigorous, fundamental scheme for the study of general non-Hermitian quasicrystals with both a complex phase factor and nonreciprocal hopping. Specially, the localization-delocalization transition point, the $\mathcal{PT}$-symmetry-breaking point, and the winding number transition points are determined by LEs of its dual Hermitian model. The analysis was based on Avila's global theory, and we found that the winding number is directly related to the acceleration and the slope of the LE, while quantization of acceleration is the crucial ingredient of Avila's global theory. This result applies as well to models with higher winding, not only the simplest Aubry-André model. As typical examples, we obtain the analytical phase boundaries of the localization transition for the non-Hermitian Aubry-André model in the whole parameter space, and the complete phase diagram is straightforwardly determined. For the non-Hermitian Soukoulis-Economou model, a high winding model, we show how the phase boundaries of the localization transition and winding number transitions are related to the LEs of its dual Hermitian model. Moreover, we discover an intriguing feature of the robust spectrum, i.e., the spectrum remains invariant when one changes the complex phase parameter h or the nonreciprocal parameter g in the region of $h < |h_c|$ or $g < |g_c|$ if the system is in the extended or localized state, respectively.

I. INTRODUCTION

Localization induced by disorder is an old but enduring research topic in condensed-matter physics [1]. While Anderson localization induced by random disorder has been studied thoroughly [2–5], the localization transition in quasiperiodic systems has attracted increasing interest in recent years [6–10]. In comparison with random disorder systems, quasiperiodic systems manifest some peculiar properties and may support exact results due to the existence of duality relation for the transformation between lattice and momentum spaces. A typical example is the Aubry-André (AA) model [8], which undergoes a localization transition when the quasiperiodic potential strength exceeds a transition point determined by a self-duality condition [11]. Various extensions of AA models have been studied [10,12–19]. The quasiperiodic lattice models can support energy-dependent mobility edges when either short-range (long-range) hopping processes [20–26] or modified quasiperiodic potentials [27–29] are introduced.

The interplay of non-Hermiticity and disorder brings a new perspective for the localization phenomena. Due to the release of the Hermiticity constraint, non-Hermitian random matrices contain much richer symmetry classes according to

Bernard-LeClair classification [30–33] than the corresponding Hermitian Altland-Zirnbauer classification. In the scheme of random matrix theory, it has been demonstrated that the spectral statistics for non-Hermitian disorder systems displays many different features from the Hermitian systems [34–41]. The interplay of the nonreciprocal hopping and random disorder has been studied in terms of the Hatano-Nelson-type models [42–47]. The effect of complex disorder potentials has also been investigated [48–50]. Non-Hermitian quasiperiodic systems have also attracted intensive studies very recently [51–67].

The LE is an important quantity to characterize the localization properties of disorder systems, and it plays an essential role in the study of the localization transition. As part of Avila's Fields Medal work, he developed a global theory of quasiperiodic cocycles, and he studied the delicate but fundamental property of LE. This is quite important progress in the spectral theory of self-adjoint quasiperiodic Schrödinger operators [68,69]. Nevertheless, the application of the global theory to the study of physical properties of quasiperiodic systems is not well recognized in the physics communities. In particular, the study of non-Hermitian quasicrystals in terms of global theory was only addressed very recently [61], and a systematic scheme applicable for general non-Hermitian quasiperiodic systems has not been established yet. The studies of the general non-Hermitian quasiperiodic models with high winding number are neglected due to the lack of exact transition points and universal formulas. In this paper, we

*qizhou@nankai.edu.cn
†schen@iphy.ac.cn

develop a fundamental scheme for the study of general non-Hermitian quasiperiodic systems by applying Avila's global theory, where the non-Hermitian systems can be realized by introducing both nonreciprocal hopping and a complex phase factor in the Hermitian quasiperiodic model. We find some universal results to determine the localization-delocalization transition point, the $\mathcal{PT}$-symmetry-breaking point, and the winding number transition points. In the presence of a complex phase factor, the picture of LE actually gives us the mechanism of how a winding number and a localized phase change with a complex phase factor. It is surprising that the relevant information for the non-Hermitian systems can be acquired from their dual Hermitian models. In the presence of nonreciprocal hopping, the skin effect–localization transition and the winding number transition are also directly related to LEs.

We stress that our theory and formalism are valid for general non-Hermitian quasiperiodic systems. For a better understanding, our general theory is made concrete by focusing on two typical examples, i.e., the non-Hermitian AA model and the Soukoulis-Economou model, as showcases for presenting the main results. Despite its deceptively simple form, the phase boundaries of the localization-delocalization transition of the general non-Hermitian AA model are still not known, except for two limit cases in the absence of either nonreciprocal hopping [55] or a complex potential [56]. A complete phase diagram with analytical phase boundaries in the full parameter space is lacking. In addition, although the coincidence of the localization transition point with the the $\mathcal{PT}$-symmetry-breaking point in the $\mathcal{PT}$-symmetry AA model has been numerically observed [55], no analytical proof is given. We shall clarify these issues by applying our general scheme. Some unusual and unexplored spectrum features of non-Hermitian AA models, i.e., the spectra are invariant with the change of complex phase parameter h or nonreciprocal parameter g in specific regions, are also unveiled. The feature of robust spectra is found to exist very commonly in non-Hermitian quasiperiodic systems.

The paper is organized as follows. In Sec. II, we first introduce the general model and we present the formalism of our general theory. We start from the systems with a complex quasiperiodic potential in the Sec. II A, and we demonstrate that the localization-delocalization transition point for general non-Hermitian quasicrystals with a complex phase factor can be determined by the LEs of its dual Hermitian model. Under the general framework, both the complex AA model and the Soukoulis-Economou model are studied. Then we study the general case in the presence of nonreciprocal hopping in Sec. II B. Taking the non-Hermitian AA model as a typical example, we obtain the complete phase diagram, which is determined by an analytical formula for the localization transition point. In Sec. III, We study the properties of winding numbers and we relate them directly to the slope of LEs. Then we identify that the phase diagram of non-Hermitian quasiperiodic models can be characterized by winding numbers. In Sec. IV, we study the properties of the robust spectrum and the skin effect. The invariance of the spectrum structure of the non-Hermitian AA model under the change of h or g in specific regions is studied and analyzed. Then we study the interplay of the skin effect and localization, and we demon-

strate that the sensitivity of the spectrum structures to the change of the boundary condition from periodic to open (PBC to OBC) can distinguish the skin and localized phases. In Sec. V, we give some examples beyond the AA model and the Soukoulis-Economou model. A summary is given in the final section.

II. MODELS AND GENERAL THEORY

We consider the general non-Hermitian quasiperiodic models with both a complex potential and nonreciprocal hopping, described by

$$H = \sum_{j=1}^{N} (t_L |j\rangle\langle j+1| + t_R |j+1\rangle\langle j| + V_j |j\rangle\langle j|), \quad (1)$$

where $t_L = t e^{-g}$ and $t_R = t e^{g}$ are the left-hopping and right-hopping amplitude, respectively, V_j is given by

$$V_j = \sum_{l=1}^{d} 2\lambda_l \cos[l(2\pi\omega j + \theta)], \quad (2)$$

with

$$\theta = \phi + ih$$

describing a complex phase factor, and N is the lattice size. For convenience, we set $t = 1$ as the unit of energy and we take $\omega = (\sqrt{5} - 1)/2$, which can be approached by $\omega = \lim_{n\to\infty} \frac{F_{n-1}}{F_n}$ with the Fibonacci numbers F_n defined recursively by $F_{n+1} = F_n + F_{n-1}$ and $F_0 = F_1 = 1$. By taking $|\psi\rangle = \sum_j u_j |j\rangle$, the eigenequation is given by

$$E u_j = e^{-g} u_{j+1} + e^{g} u_{j-1} + V_j u_j, \quad (3)$$

where the eigenvalue E is generally complex.

A. Models with a complex quasiperiodic potential

We first discuss the case in the absence of nonreciprocal hopping, i.e., $g = 0$. For $\phi = 0$, we have $V_j = V_{-j}^*$; the model (1) with $g = 0$ has $\mathcal{PT}$ symmetry [52,70]. Our whole analysis depends on Avila's global theory of a quasiperiodic Schrödinger operator [68] (see Appendix A for a brief introduction), where the key is to analyze the LE $\gamma(E, h)$ with respect to h. The LE is given by

$$\gamma(E) = \lim_{n\to\infty} \frac{1}{n} \ln ||T_n(E)||, \quad (4)$$

where the transfer matrix

$$T_n(E) = \prod_{j=1}^{n} T^j = \prod_{j=1}^{n} \begin{pmatrix} E - V_j & -1 \\ 1 & 0 \end{pmatrix} \quad (5)$$

and $||A||$ represents the norm of the matrix A, defined by

$$||A|| = \max_{i=1:n} \sqrt{\lambda_i(A^T A)},$$

with $\lambda_i(A^T A)$ being the ith eigenvalue of $A^T A$.

As shown in [68], $\gamma(E, h)$ is a convex and piecewise linear function with respect to h with their slopes being integers.

If V_j is a trigonometric polynomial (i.e., $d < \infty$), then the extreme points of $\gamma(E, h)$ can be determined by the LE of

$$
\gamma(E, h) =
\begin{cases}
\gamma(E, 0), & h \in [0, \chi_1(E)], \\
\vdots & \vdots \\
\gamma(E, \chi_i(E)) + [h - \chi_i(E)] \sum_{j=1}^{i} n_j, & h \in (\chi_i(E), \chi_{i+1}(E)], \\
\vdots & \vdots \\
\gamma(E, \chi_\ell(E)) + [h - \chi_l(E)] \sum_{j=1}^{\ell} n_j, & h \in (\chi_\ell(E), \infty),
\end{cases}
\tag{6}
$$

where $0 \leqslant \chi_1(E) < \cdots < \chi_\ell(E)$ are the non-negative LEs with multiplicity $n_1, \ldots, n_\ell$ for the dual model of the system (1) with $h = 0$,

$$
E\tilde{u}_k = \sum_{l=-d}^{d} \lambda_{|l|} \tilde{u}_{k+l} + 2\cos(2\pi\omega k)\tilde{u}_k. \tag{7}
$$

This means that the LE $\gamma(E, h)$ can be uniquely determined by $\gamma(E, 0)$, χ_i, and n_i. These points $h = \chi_i$ are knotted, corresponding to some physical consequence. However, we emphasize that duality is not the essence of our approach. The crucial elements are the extreme point and the slope of $\gamma(E, h)$, and duality only provides an efficient way to achieve these parameters. That is also the reason why our approach works for general non-Hermitian quasiperiodic models (cf. Sec. V). We should also point out that in the following discussion, we only need to consider the case E belonging to the spectrum of the Hermitian case ($h = 0$). Actually, based on Avila's global theory, we can see that if E does not belong to the spectrum of the Hermitian case, $\gamma(E, 0) > 0$ and $\chi_1(E) > 0$. To better understand Eq. (6), we show the LE $\gamma(E, h)$ in Figs. 1(a) and 1(b) as a function of h with $h > 0$. Note that $\gamma(E, h)$ is symmetric over h, i.e.,

$$
\gamma(E, h) = \gamma(E, -h). \tag{8}
$$

An intriguing issue is that the $\mathcal{PT}$-symmetry-breaking transition and the transition from extended to localized states can both be determined by the LE of the Hermitian dual model $\chi_1(E)$. To explain it clearly, we will start with a representative model, namely the AA model, i.e., only $\lambda_1 \neq 0$, which is discussed in detail in the following. The dual model form for the model (1) with $g = 0$, $h = 0$, and $\lambda_{l \geqslant 2} = 0$ is

$$
E\tilde{u}_k = \lambda_1 \tilde{u}_{k+1} + \lambda_1 \tilde{u}_{k-1} + 2\cos(2\pi\omega k)\tilde{u}_k. \tag{9}
$$

The exact LE $\chi(E)$ of this dual model can be obtained by Eq. (4) with the transfer matrix T_n given by

$$
T_n(E) = \prod_{j=1}^{n} T^j = \prod_{j=1}^{n} \begin{pmatrix} \frac{E - 2\cos(2\pi\omega k)}{\lambda_1} & -1 \\ 1 & 0 \end{pmatrix}. \tag{10}
$$

From the discussions in [29,68], we have

$$
\chi(E) = \max\{-\ln|\lambda_1|, 0\} \tag{11}
$$

if the energy E belongs to the spectrum. Thus the LE for the original model with $h \neq 0$ can be written as

$$
\gamma(E, h) =
\begin{cases}
\gamma(E, 0), & h \in (0, \chi(E)), \\
\gamma(E, \chi(E)) + [h - \chi(E)], & h \in (\chi(E), \infty),
\end{cases}
\tag{12}
$$

the corresponding dual Hermitian Hamiltonian [71]. More precisely, it has the following expansion:

$$
\qquad\qquad\qquad h \in [0, \chi_1(E)],
$$
$$
\vdots
$$

which can also be rewritten as

$$
\gamma(E, h) = \max\{\ln|\lambda_1| + |h|, 0\}. \tag{13}
$$

The LE can also be directly derived from the original model (see Appendix A 1) without the need to introduce the dual model.

Figures 1(c) and 1(d) show the LE $\gamma(E, h)$ for noncritical AA models with $|\lambda_1| < 1$ and $|\lambda_1| > 1$, respectively. Note that $\gamma(E, h) = 0$ indicates the extended state, and $\gamma(E, h) > 0$ corresponds to the localized state. Thus if $|\lambda_1| < 1$, all the eigenstates of the Hermitian AA model ($h = 0$) are extended. When $|h| > 0$, there exists a localization-delocalization transition point determined by

$$
|h| = -\ln|\lambda_1|. \tag{14}
$$

If $|\lambda_1| > 1$, all the eigenstates of the Hermitian AA model are localized and all the eigenstates stay localized with $|h| > 0$.

In the following, we first consider the case $|\lambda_1| < 1$. For simplicity, we only discuss the case $h > 0$. According to Avila's global theory [68], E does not lie in the spectrum
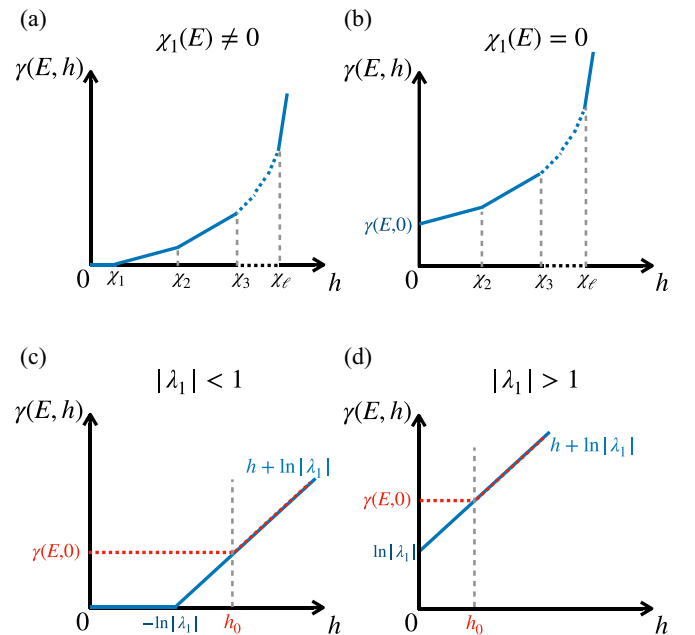
FIG. 1. Schematic representation of Eq. (6): the LE $\gamma(E, h)$ as a function of h for (a) $\chi \neq 0$ and (b) $\chi = 0$, respectively. For the AA model, the LE $\gamma(E, h)$ with (c) $|\lambda_1| < 1$ and (d) $|\lambda_1| > 1$, respectively.

of the Hamiltonian $h = h_0$ if and only if $\gamma(E, h_0) > 0$, and $\gamma(E, h)$ is a linear function around h_0. Therefore, if E lies in the spectrum of the Hermitian case $h = 0$, it belongs to the spectrum of the system with $h < -\ln|\lambda_1|$, but it does not belong to the spectrum of the system with $h > -\ln|\lambda_1|$, as shown by the blue dashed line in Fig. 1(c). Conversely, if the energy E (which might be complex) does not lie in the spectrum of the Hermitian case $h = 0$, then $\gamma(E, 0) > 0$, and $\gamma(E, h)$ is locally constant in h, as shown by the red dashed line in Fig. 1(c). Note that h_0 is an extreme point of $\gamma(E, h)$ if and only if $h_0 > -\ln|\lambda_1|$. Therefore, these energies E do not belong to the spectrum of the system with $h < -\ln|\lambda_1|$, but they might belong to the spectrum of the system with $h > -\ln|\lambda_1|$. By the above discussions, we prove that the extended states have real energies when $h < -\ln|\lambda_1|$, and the localized states have complex eigenvalues when $h > -\ln|\lambda_1|$. This explains why the localization-transition point coincides with the $\mathcal{PT}$-symmetry-breaking point. Furthermore, the spectrum remains invariant in the regime of extended states, which is indeed a Cantor set by the famous result of Avila-Jitomirskaya [72].

However, the case $|\lambda_1| > 1$ will be much simpler. Similar to what was discussed above, one can easily deduce that when $h > 0$, all the states that have complex eigenvalues are localized, as shown in Fig. 1(d).

To get a straightforward understanding, next we demonstrate the numerical results of LE, the inverse participation ratio (IPR), the normalized participation ratio (NPR) [23–25], and the energy spectrum as a function of h. For a finite system, the LE can be numerically calculated via

$$\gamma(E) = \ln\left(\max\left(\theta_i^+, \theta_i^-\right)\right), \quad (15)$$

where $\theta_i^\pm \in \mathbb{R}$ denote eigenvalues of the matrix

$$\boldsymbol{\Theta} = (T_N^\dagger T_N)^{1/(2N)}. \quad (16)$$

The IPR and NPR of an eigenstate are defined as

$$\mathrm{IPR}^{(n)} = \left(\sum_j |u_j^n|^4\right) \Big/ \left(\sum_j |u_j^n|^2\right)^2$$

and

$$\mathrm{NPR}^{(n)} = \left[N \sum_i |u_i^n|^4\right]^{-1}, \quad (17)$$

where the superscript n labels the nth eigenstate of the system, and j represents the lattice coordinate. For an extended eigenstate, $\mathrm{IPR} \simeq 1/N$ approaches zero as $N \to \infty$ and NPR is a finite value. On the other hand, $\mathrm{IPR} \simeq 1$ and $\mathrm{NPR} \simeq 0$ for a full localized eigenstate.

Figures 2(a) and 2(c) show the numerical results of the LE and IPR versus h, respectively. If $|\lambda_1| < 1$, when $|h| < \chi(E)$, where $\chi(E) = -\ln|\lambda_1| \approx 0.7$ for $\lambda_1 = 0.5$, all eigenstates are extended states and both LE and IPR approach zero. On the other hand, when $h > \chi(E)$, both LE and IPR have a sudden increase. If $|\lambda_1| > 1$, all eigenstates are localized, as shown in Fig. 2(a) with $\lambda_1 = 2$. The numerical results of LE for a finite-size system are found to agree well with the analytical result (13). In Fig. 2(b), we display the real
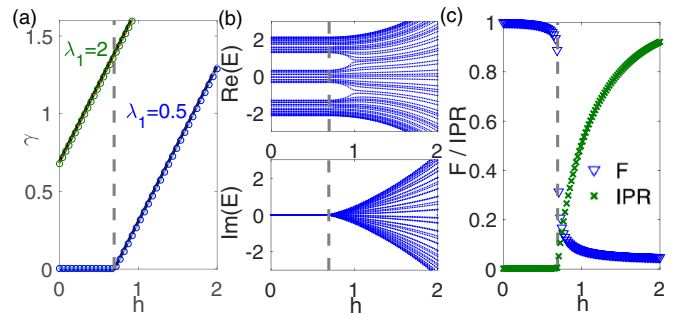
FIG. 2. (a) Numerical results for the LE of eigenstates corresponding to the minimum (circles) and maximum (dots) real part of eigenvalues Re(E) vs h for the system with $g = 0$, $N = 1597$, and $\lambda = 0.5$ and 2, respectively. The black solid lines represent the exact solution of the LE obtained by (13). (b) The real and the imaginary part of the eigenvalue spectra vs h for the system with $\lambda_1 = 0.5$, $g = 0$, and $N = 55$. (c) The fidelity F and IPR of the eigenstate corresponding to the minimum real part of eigenvalues Re(E) vs h for the system with $g = 0$, $N = 1597$, and $\lambda_1 = 0.5$.

and imaginary parts of eigenvalues versus h for the system with $\lambda_1 = 0.5$. While all eigenvalues are real for $h < \chi(E)$, they become complex when h exceeds $\chi(E)$. This clearly shows that the transition from extended to localized states and the $\mathcal{PT}$-symmetry breaking transition have the same boundary.

It is also interesting to notice that the spectrum does not change with h in the extended region as long as $h < \chi(E)$. This kind of phenomenon is quite unusual, since the Hamiltonian with different h is not unitarily equivalent, and it is just a kind of *robust spectrum*. The similarity of two eigenstates can be characterized by the fidelity

$$F(h) = \langle \psi_g(0) | \psi_g(h) \rangle, \quad (18)$$

where $\psi_g(h)$ is the eigenstate of the corresponding minimum real part of the eigenvalue, and $\psi_g(0)$ with $h = 0$. The eigenstates vary only slightly from $h = 0$ to $h < \chi(E)$, and they change suddenly at the transition point $h = \chi(E)$, as shown in Fig. 2(c).

Although the above phenomena occur in a simple case, they can be commonly found in general non-Hermitian quasiperiodic models (1) with $g = 0$. If $\chi_1(E) = 0$, which means $\gamma(E, 0) > 0$, there is no extended-localized transition for the complex phase $h > 0$. We thus only need to consider the case $\chi_1(E) > 0$. If $0 < h < \chi_1(E)$ for a given eigenvalue E of the system with $h = 0$, the eigenvalue remains unchanged and the corresponding eigenstate is extended. If $h > \chi_1(E)$, the eigenvalue becomes complex and the corresponding eigenstate is localized. As a consequence, $h = \min\{\chi_1(E)\}$ gives the beginning of $\mathcal{PT}$-symmetry breaking and the extended-mixed transition, while $h = \max\{\chi_1(E)\}$ gives us the mixed-localized transition. That is to say, if $\min\{\chi_1(E)\} < h < \max\{\chi_1(E)\}$, the mobility edges will occur, the spectrum will have both real and complex energies, and the phases will be a mixture of extended and localized states. Moreover, if $0 < h < \min\{\chi_1(E)\}$, the spectrum is exactly the same as the Hermitian case $h = 0$, thus it has a robust spectrum with changing h. Just note that if $\min\{\chi_1(E)\} =$

$\max\{\chi_1(E)\}$ or say $\chi_1(E)$ is a constant, then $h = \min\{\chi_1(E)\}$ gives the extended-localized transition point, as in the non-Hermitian AA model. Finally, we point out that $\chi_1(E)$ is also the inverse of the localization length of the eigenstate for the Hermitian dual model (7), and if $\chi_1(E) > 0$, the corresponding eigenstate of system (7) is localized.

Next we will demonstrate this with the Soukoulis-Economou model [73], one of the first proposals of one-dimensional quasiperiodic models containing single-particle mobility edges. It is a tight-binding model with nearest-neighbor hopping terms as well as two quasiperiodic on-site potentials:

$$V_j = 2\lambda_1 \cos(2\pi\omega j + ih) + 2\lambda_2 \cos(4\pi\omega j + 2ih). \quad (19)$$

Our analysis shows that the mobility edge for the system with any h can be determined by the LE $\chi_1(E)$ for its dual Hermitian system (7).

For the potential (19) with $h = 0$, its dual model (7) is

$$E\tilde{u}_k = \lambda_1(\tilde{u}_{k+1} + \tilde{u}_{k-1}) + \lambda_2(\tilde{u}_{k+2} + \tilde{u}_{k-2}) + 2\cos(2\pi\omega k)\tilde{u}_k \quad (20)$$

and $\tilde{u}_k = \sum_n e^{-i2\pi\omega kj} u_j$. We can rewrite (20) as

$$\begin{pmatrix} \tilde{u}_{k+3} \\ \tilde{u}_{k+2} \\ \tilde{u}_{k+1} \\ \tilde{u}_k \end{pmatrix} = T^k \begin{pmatrix} \tilde{u}_{k+1} \\ \tilde{u}_k \\ \tilde{u}_{k-1} \\ \tilde{u}_{k-2} \end{pmatrix},$$

with

$$T^k = \begin{pmatrix} C_2^{-1}(EI_2 - B_2) & -C_2^{-1}C_2^* \\ I_2 & 0 \end{pmatrix},$$

where I_2 is the 2×2 identity matrix, and the matrices C_2 and B_2 are given by

$$C_2 = \begin{pmatrix} \lambda_2 & \lambda_1 \\ 0 & \lambda_2 \end{pmatrix}$$

and

$$B_2 = \begin{pmatrix} 2\cos(2\pi\omega(k+1)) & \lambda_1 \\ \lambda_1 & 2\cos(2\pi\omega k) \end{pmatrix}.$$

If we denote the transfer matrix $T_n(E) = \prod_k T^k$, then the LEs of the model (20) are given by

$$\chi_i = \ln\theta_i, \quad (21)$$

where θ_i are the eigenvalues of the matrix,

$$\Theta = \left(T_N^\dagger T_N\right)^{1/(2N)}.$$

Since T^k is a 4×4 complex symplectic matrix, their LEs (21) come in pairs, and we write it as $-\chi_2(E) \leqslant -\chi_1(E) \leqslant 0 \leqslant \chi_1(E) \leqslant \chi_2(E)$. The LE (6) for the original model with $d = 2$ and $h \neq 0$ can be written as

$$\gamma(E, h) = \begin{cases} \gamma(E, 0), & h \in [0, \chi_1(E)], \\ \gamma(E, \chi_1(E)) + [h - \chi_1(E)], & h \in (\chi_1(E), \chi_2(E)], \\ \gamma(E, \chi_2(E)) + 2[h - \chi_2(E)], & h \in (\chi_2(E), \infty). \end{cases} \quad (22)$$

Figure 3(a) shows the LEs $\chi_1(E)$ and $\chi_2(E)$ of the dual model (20) with $\lambda_1 = 0.2$ and $\lambda_2 = 0.25$ as a function of eigenenergy E, and in Figs. 3(b) and 3(c) we display its spectrum versus h. We also show the averaged IPR and NPR in Fig. 3(d) to distinguish these phases. From these pictures, it is clear that the spectrum remains invariant in the region of $h < h_1$, where $h_1 = \min\{\chi_1(E)\} = 0.23$ is also the $\mathcal{PT}$-symmetry-breaking point, all the eigenvalues are real, and all the eigenstates are extended. The mobility edge region $h_1 < h < h_2$ represents the system with a mixture of localized and extended states, where $h_2 = \max\{\chi_1(E)\} = 0.6$. The extended states have real eigenvalues, while the localized states have complex eigenvalues, as shown in Figs. 3(b3) and 3(c). Eventually, when $h > h_2$, all the eigenstates are localized, and their corresponding eigenvalues are complex. Our results clearly indicate that the three distinct phases can be divided by $h = \max\{\chi_1(E)\}$ and $h = \max\{\chi_1(E)\}$.

B. Effect of nonreciprocal hopping

Now we consider the general case with $g \neq 0$. The non-reciprocal hopping breaks the $\mathcal{PT}$ symmetry and may induce the skin effect under OBC. The Hamiltonian $H(g)$ under OBC can be transformed to H' via a similar transformation,

$$H' = SH(g)S^{-1}, \quad (23)$$

where

$$S = \text{diag}(e^{-g}, e^{-2g}, \ldots, e^{-Ng})$$

is a similarity matrix with only diagonal entries, and $H' = H(g = 0)$ is the Hamiltonian with $g = 0$. The eigenvectors of H and H' satisfy $|\psi\rangle = S^{-1}|\psi'\rangle$. An extended state $|\psi'\rangle$ under the transformation S^{-1} becomes skin states, which exponentially accumulate to one of the boundaries [56,74–78].

A localized state of H' generally takes the following form:

$$|u_i| \propto e^{-|i-i_0|/\xi},$$

where i_0 represents the position of the localization center of a given localized state, $\xi = 1/\gamma$ is the localization length, and γ is the LE of the localized state for the system with $g = 0$. Then the corresponding wave function of $H(g)$ takes the following
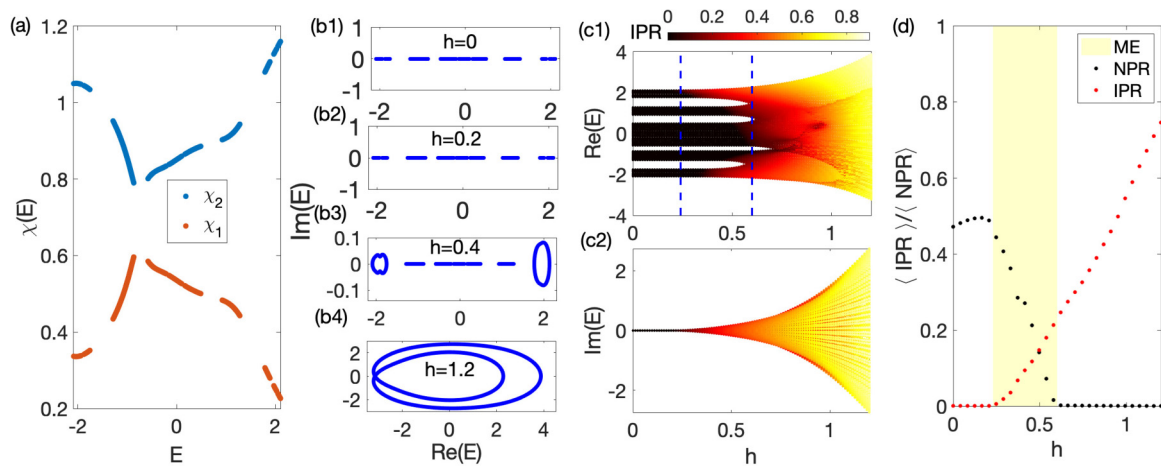
FIG. 3. (a) The LE of the dual model with $\lambda_1 = 0.2$ and $\lambda_2 = 0.25$. (b) The complex spectrum for systems with (b1) $h = 0$, (b2) 0.2, (b3) 0.4, and (b4) 1.1, respectively. (c) The real and imaginary part of the eigenvalue spectra vs h for the system with $g = 0$, $\lambda_1 = 0.2$, and $\lambda_2 = 0.25$. Dashed blue lines indicate the transition point: $h_1 = 0.23$ and $h_2 = 0.6$. (d) Averaged IPR and NPR for all eigenstates in the model.

form:

$$|u_i| \propto \begin{cases} e^{-(\gamma-g)|i-i_0|}, & i > i_0, \\ e^{-(\gamma+g)|i-i_0|}, & i < i_0, \end{cases} \tag{24}$$

which has different decaying behaviors on different sides of the localization center. When $|g| \geqslant \gamma$, delocalization occurs on one side and then the skin state emerges to the boundary. The transition point from the localized state to the skin state is given by

$$\gamma(E) = |g|. \tag{25}$$

Since a localized state is not sensitive to the boundary condition of the system, we conclude that the boundary of the localization-delocalization transition under the PBC is also given by Eq. (25).

For the general Hermitian quasiperiodic model (1), LEs might depend on E, and a mobility edge will occur. Consequently, if $g \neq 0$, Eq. (25) gives the mobility edge from the localized state to the extended (skin) state. The localized eigenstate in the case $g = 0$ is still localized when $0 < g < \gamma(E)$. However, the localized eigenstate becomes extended (skin) under the PBC (OBC) when $g > \gamma(E)$.

For the non-Hermitian AA model with $h \neq 0$ and $g = 0$, the LEs of the localized states are given by $\gamma = |h| + \ln|\lambda_1|$ according to Eq. (13). Thus if $g \neq 0$, by using Eq. (25), the localization-transition boundary is determined by

$$|h| + \ln|\lambda_1| = |g|, \tag{26}$$

which can be alternatively represented as

$$|\lambda_1| = e^{-|h|+|g|}. \tag{27}$$

While all eigenstates are localized for $|\lambda_1| > e^{-|h|+|g|}$, they become extended (skin) states under PBC (OBC) for $|\lambda_1| < e^{-|h|+|g|}$. The model reduces to the classical AA model when $h = 0$ and $g = 0$. Equation (27) recovers the result of Ref. [55] for $h \neq 0$ and $g = 0$ and the result of Ref. [56] for $g \neq 0$ and $h = 0$.

By using either Eq. (26) or Eq. (27), we can obtain the complete phase diagram. For a given λ_1, we display the phase diagram in Fig. 4 with the phase boundaries (solid lines) determined by Eq. (26). Figures 4(a) and 4(b) correspond to the case $\lambda_1 < 1$ and $\lambda_1 > 1$, respectively. Here regions labeled by A denote the Anderson localized phase, and regions labeled by L or R represent the left or right skin states under OBC, which are an extended phase under PBC. From the phase diagrams, we can see that, while increasing $|h|$ tends to drive the system into the localized phase, increasing $|g|$ tends to drive the system into the extended (skin) phase. When $|h| = |g|$, the transition point is given by $\lambda_c = 1$, which is irrelevant to the values of h and g, and the eigenstates for the system with $\lambda_1 < 1$ ($\lambda_1 > 1$) are extended (localized).

For the AA model, the LE of the localized state is independent of E. This suggests that all eigenstates are either localized
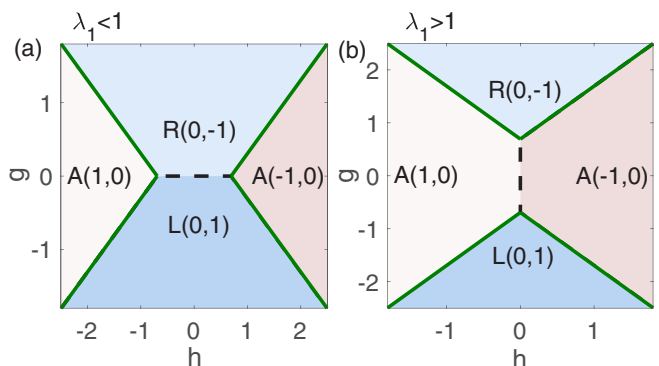
FIG. 4. Phase diagrams for the case with (a) $|\lambda_1| < 1$ and (b) $|\lambda_1| > 1$, respectively. The phase boundaries are denoted by the green solid lines, which are determined by $|g| = \ln|\lambda_1| + |h|$. The winding numbers (ν_ϕ, ν_ψ) are defined in the text. $\{L, R, A\}$ represent the left-skin, right-skin, and Anderson localized phases, respectively. The left-skin and right-skin phases under OBC correspond to extended phases under PBC. We have taken $\lambda_1 = 0.5$ in (a) and $\lambda_1 = 2$ in (b).
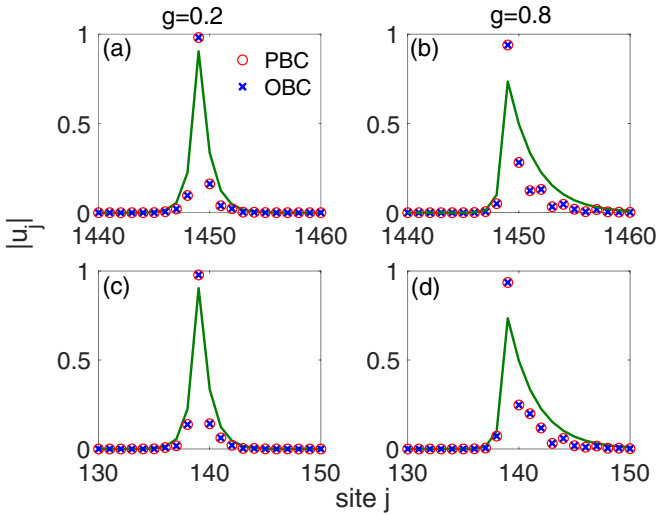
FIG. 5. The distribution of eigenstates for systems with $\lambda_1 = 2$, $h = 0.5$, $N = 1597$, $g = 0.2$, and 0.8, respectively. The red circles and blue crosses represent the eigenvalues under PBC and OBC, respectively. The solid line is plotted by using Eq. (24). The localization centers for states shown in (a) and (b) are at $j = 1449$, and for (c) and (d) they are at $j = 139$.

or extended (skin) states with the transition point independent of E. Also, we can conclude that all localized states of the non-Hermitian AA model can be described by a unified wave function (24) with different states having different localization centers, as shown in Figs. 5(a) and 5(c) or Figs. 5(b) and 5(d).

III. WINDING NUMBERS

The phase factor ϕ of the potential provides a parameter space to define the topological invariant, i.e., the winding number, to characterize the topological phase of the non-Hermitian quasiperiodic system. Changing the complex phase h may induce a topological phase transition. Recall that the winding number of the system can be defined as

$$\nu_\phi = \frac{1}{2\pi i} \frac{1}{N} \int_0^{2\pi} d\phi \, \partial_\phi \ln \det[H(\phi) - E_B], \qquad (28)$$

which measures the change of the spectrum with respect to the base energy E_B when ϕ is changed continuously. Thus an interesting question is, where does the topological transition occur? Indeed, this question can also be answered with the help of LE. As we explained above, the slope of LE, which is called acceleration [68], is quantized. We will show that *quantization of the winding number just means that the acceleration is quantized.*

Let us explain in more detail. In the case $g = 0$, as we show in Appendix B, based on the Cauchy-Riemann equation, we have the following relation:

$$\nu_\phi(E, h) = -\frac{\partial \gamma(E, h)}{\partial h}. \qquad (29)$$

Here $\frac{\partial \gamma(E,h)}{\partial h}$ is exactly the "acceleration" as defined by Avila [68]. Note that $\gamma(E, h)$ is a piecewise linear function with respect to h with their slopes being integers, and then acceleration is just the slope. In the following sections, we only need
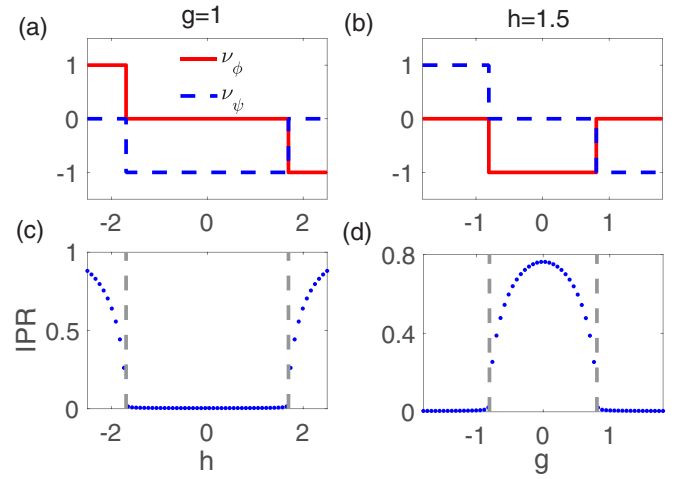
FIG. 6. The winding number ν_ϕ, ν_ψ vs h for the system with $g = 1$ (a) and vs g for the system with $h = 1.5$ (b). The IPR of eigenstates corresponding to the middlemost real part of eigenvalue Re(E) vs h for the system with $g = 1$ (c) and vs g for the system with $h = 1.5$ (d). Other parameters are $\lambda_1 = 0.5$ and $N = 233$, and we have taken PBC in the numerical calculations.

to consider $h > 0$. Due to the symmetry (8), $\nu_\phi(E, h)$ always satisfies

$$\nu_\phi(E, -h) = -\nu_\phi(E, h). \qquad (30)$$

If $g \neq 0$, then boundary conditions make things different. Under PBC, we will show that

$$\nu_\phi(E, h, g) = \begin{cases} 0, & |g| > \gamma(E, h), \\ -\frac{\partial \gamma(E,h)}{\partial h}, & 0 < |g| < \gamma(E, h). \end{cases} \qquad (31)$$

However, within OBC, we have

$$\nu_\phi(E, h, g) = \nu_\phi(E, h) = -\frac{\partial \gamma(E, h)}{\partial h} \qquad (32)$$

for any $g \neq 0$. Equations (31) and (32) are strictly evoked in Appendix B. The different boundary conditions correspond to the different winding number, which can also be interpreted as a phenomenon for the breakdown of bulk-boundary correspondence.

Based on Eqs. (6), (29), and (31), our analysis really shows the topological transition of general non-Hermitian quasiperiodic models, that is to say, the transition point is also determined by the LE $\chi_i(E)$ of the dual model (7). For simplicity, we will just demonstrate this with the AA model and the Soukoulis-Economou model.

For the non-Hermitian AA model, when $\lambda_1 < 1$, Eqs. (29) and (31) can be expressed as

$$\nu_\phi(E, h) = \begin{cases} 0, & h < -\ln |\lambda_1|, \\ -1, & h > -\ln |\lambda_1| \end{cases} \qquad (33)$$

and

$$\nu_\phi(E, h, g) = \begin{cases} 0, & g > h + \ln |\lambda_1|, \\ -1, & g < h + \ln |\lambda_1|, \end{cases} \qquad (34)$$

based on Eq. (13). In Fig. 6, we show how the winding numbers and IPR change with h or g. Figures 6(a) and 6(c) are for the system with fixed $\lambda_1 = 0.5$ and $g = 1$. According

(a)

$\nu_\phi(E_B)$	0	0,-1	-1	-1,-2	-2

0 min$\{\chi_1(E)\}$ max$\{\chi_1(E)\}$ min$\{\chi_2(E)\}$ max$\{\chi_2(E)\}$ h

Spectrum	real	real, complex	complex
Phase (PBC)	extended	mixed	localized
Phase (OBC)	Skin	mixed	localized

* *Note that we chose the eigenvalues of the system with $h = 0$ as the base energies E_B.*
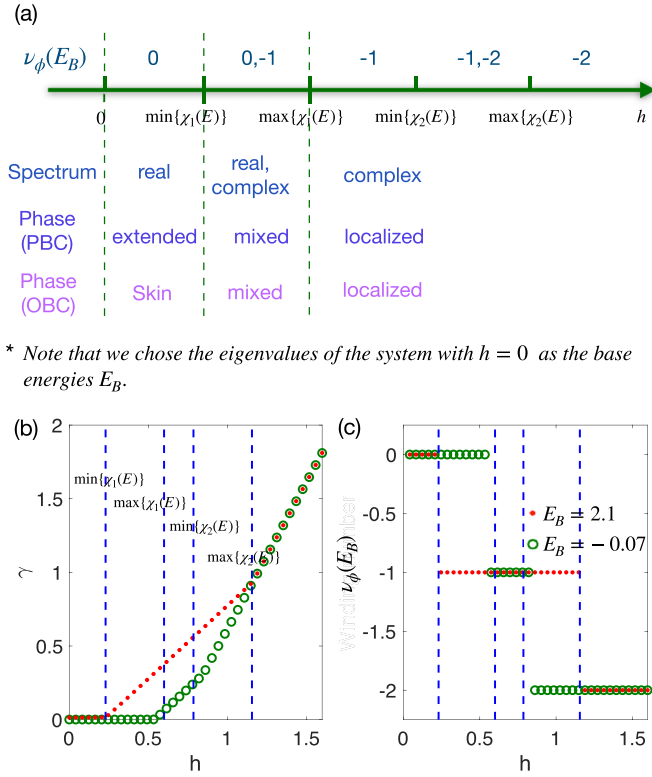
FIG. 7. (a) The winding numbers ν_ϕ, spectrum, and phases for the system with potential (19) and $g = 0$ vs h, which is associated with the minimum and maximum values of $\chi_{1,2}(E)$. Numerical results for the LE (b) and the winding numbers ν_ϕ (c) of systems with $\lambda_1 = 0.2$, $\lambda_2 = 0.25$, $g = 0$, and $E_B = -0.071$ and 2.1 vs h. For this case, the minimum and maximum values of $\chi_{1,2}(E)$ are min$\{\chi_1(E)\} = 0.23$, max$\{\chi_1(E)\} = 0.6$, min$\{\chi_2(E)\} = 0.786$, and max$\{\chi_2(E)\} = 1.156$, respectively.

to Eq. (25), we have $|h_c| = |g| - \ln|\lambda_1| \approx 1.7$. It is shown that the winding number ν_ϕ takes a different integer 0 or ± 1 in the region $|h| < 1.7$ or $|h| > 1.7$, and IPR shows that the corresponding states are extended or localized. Figures 6(b) and 6(d) show the winding numbers ν_ϕ and IPR of the system with $\lambda_1 = 0.5$ and $h = 1.5$ versus g. According to Eq. (25), we have $|g_c| = |h| + \ln|\lambda_1| \approx 0.8$. The winding number ν_ϕ takes a different integer 0 or -1 in the region $|g| < 0.8$ or >0.8, and IPR shows that the corresponding states are localized or extended. The numerical results clearly indicate that the winding number changes its value when crossing the boundary of the localization transition and it takes a different integer in the extended and localized regions. Consequently, we also show that different phases in the phase diagram of Fig. 4 can be characterized by different ν_ϕ.

Next we turn to the Soukoulis-Economou model (19). Take the eigenvalue E_B of the Hermitian system as the base energy, and substitute Eq. (22) into Eq. (29). Then one obtains its winding number when changing the parameter h:

$$\nu_\phi(E_B, h) = \begin{cases} 0, & 0 < h < \chi_1(E_B), \\ -1, & \chi_1(E) < h < \chi_2(E_B), \\ -2, & h > \chi_2(E_B). \end{cases} \quad (35)$$
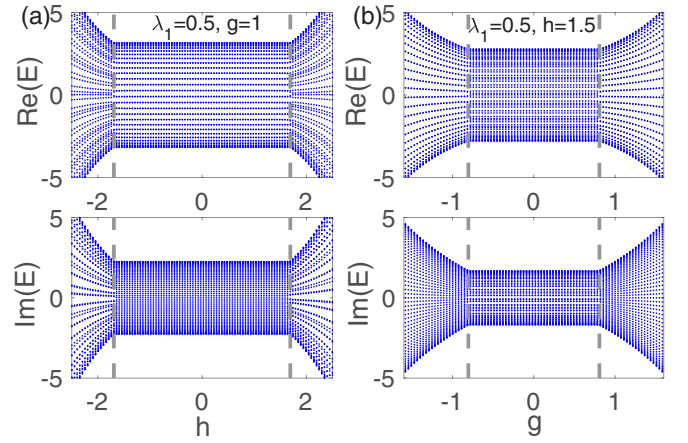
FIG. 8. (a) The real and the imaginary part of the eigenvalue spectra vs h for the AA model with $\lambda_1 = 0.5$, $g = 1$, and $N = 55$. (b) The real and imaginary part of the eigenvalue spectra vs g for the system with $\lambda_1 = 0.5$, $h = 1.5$, and $N = 55$. Dashed gray lines represent transition points.

In Fig. 7(a), we schematically display the winding number versus the change of h. Clearly, the value of the winding number depends on the choice of base energy. Figures 7(b) and 7(c) show the numerical results of the LE and winding number as a function of h with $g = 0$, $\lambda_1 = 0.2$, $\lambda_2 = 0.25$, $E_B = 2.1$, and -0.07, respectively. When $h = 0$, all eigenstates of the system are extended, thus $\gamma(E_B, 0) = 0$. It is clear that each of the LE $\gamma(E_B, h)$ is a continuous piecewise linear function with variable h and it has two extreme points, $h = \chi_1(E_B)$ and $\chi_2(E_B)$, where $\chi_{1,2}(E_B)$ are the LEs of the dual model (20), as shown in Fig. 3(a). It is obvious that the slope of the LE is zero in the region $0 < h < \chi_1(E_B)$ and the winding number $\nu_\phi(E_B, h) = 0$, all the eigenstates are extended, and all the eigenenergies are real in this region. The slope of the LE $\gamma(E_B, h)$ is 1 and the winding number $\nu_\phi(E_B, h) = -1$ in the region $\chi_1(E) < h < \chi_2(E)$. The slope of the LE $\gamma(E_B, h)$ is 2 and the winding number $\nu_\phi(E_B, h) = -2$ if $h > \chi_2(E)$. Consequently, according to min$\{\chi_{1,2}(E_B)\}$ and max$\{\chi_{1,2}(E_B)\}$, the parameter space $h > 0$ can be divided into five regions, as shown in Fig. 7(a). In the regions $0 < h < \min\{\chi_1(E_B)\}$, max$\{\chi_1(E_B)\} < h < \min\{\chi_2(E_B)\}$, and max$\{\chi_2(E_B)\} < h$, the winding numbers $\nu_\phi(E_B, h)$ are 0, 1, and 2, respectively, and they do not change with E_B. In the region min$\{\chi_1(E_B)\} < h < \max\{\chi_1(E_B)\}$, $\nu_\phi(E_B) = -1$ or 0, which depends on the selection of E_B, as shown in Fig. 8(c). Indeed, not only the winding numbers but also the states are mixed in this region. In the region min$\{\chi_2(E_B)\} < h < \max\{\chi_2(E_B)\}$, $\nu_\phi(E_B, h) = -2$ or -1, which also depends on the selection of E_B. Although the winding numbers are mixed, the states are not mixed, and all the eigenstates are localized in this region.

IV. ROBUST SPECTRUM AND SKIN EFFECT

In Sec. II, we unveiled that for general non-Hermitian quasiperiodic models (1), if all the eigenstates of the Hermitian case ($h = 0$) are extended, then the real spectrum remains invariant in the whole extended region $h < \min\{\chi_1(E)\}$, i.e., there is a robust spec-

trum. In this section, we will show that this kind of intriguing phenomenon could also happen for nonreciprocal hopping. We will demonstrate this with the AA model.

For the AA model, and the $\mathcal{PT}$-symmetric case with $g = 0$, the robust spectrum takes place in the regime $|h| < |h_c| = -\ln|\lambda_1|$. On the other hand, for the case $h = 0$, we find that the robust spectrum also occurs in the whole localized region $|g| < |g_c| = \ln|\lambda_1|$. The spectrum properties in these two limits can be understood from the observation that the two limit cases can be related by a dual transformation [56]. For the general case with $g \neq 0$ and $h \neq 0$, with the PBC, the spectrum is complex. Nevertheless, we find that the complex spectrum still remains invariant when we change h in the extended region $|h| < |h_c| = |g| - \ln|\lambda_1|$ for a fixed g or we change g in the localized region $|g| < |g_c| = |h| + \ln|\lambda_1|$ for a fixed h. To give some concrete examples, we display the spectrum for the system with $\lambda_1 = 0.5$ and $g = 1$ versus h in Fig. 8(a) and the system with $\lambda_1 = 0.5$ and $h = 1.5$ versus g in Fig. 8(b). For the case of Fig. 8(a), all eigenstates in the region of $|h| < 1.7$ are extended states, and the corresponding spectrum does not change with h as long as $|h| < 1.7$. For Fig. 8(b), all eigenstates in the region of $|g| < 0.8$ are localized states, and the corresponding spectrum does not change with g as long as $|g| < 0.8$.

Next we shall give a straightforward explanation of the robust spectrum shown in Fig. 8(b). In the region $|g| < 0.8$, the states are localized and are not sensitive to the boundary condition. Therefore, the spectra under PBC and OBC should be the same in the large size limit as long as $|g| < |g_c|$. From Eq. (23), we know that the open boundary spectrum is irrelevant with g and should be identical to the case of $g = 0$ because the similar transformation does not change the spectrum. Therefore, it is not hard to understand why the periodic boundary eigenenergies do not change with g for the localized states. When $|g| > |g_c|$, the spectra are sensitive to the boundary condition, and the corresponding states are extended or skin states under PBC or OBC.

It is not so straightforward to understand the invariance of the spectrum shown in Fig. 8(a). Nevertheless, we can give an explanation by resorting to the dual transformation. From this aspect, it is also useful to consider the ring chain with a flux penetrating through the center, yielding

$$H(\psi) = \sum_j [t_L e^{i\psi} |j\rangle\langle j+1| + t_R e^{-i\psi} |j+1\rangle\langle j| + \lambda_1 \cos(2\pi\omega j + \theta)|j\rangle\langle j|], \quad (36)$$

or equivalently by replacing the hopping term connecting the first and Nth site as $h_{1N} = t_L e^{-iN\psi}|N\rangle\langle 1| + t_R e^{iN\psi}|1\rangle\langle N|$, and the winding number is defined as

$$\nu_\psi = \frac{1}{2\pi i}\frac{1}{N}\int_0^{2\pi} d\psi \, \partial_\psi \ln\det[H(\psi) - E_B]. \quad (37)$$

ν_ψ have been utilized to characterize the loop of the energy spectra of extended and localized states [45,55,56,59].

By utilizing the dual transformation

$$|j\rangle = \frac{1}{\sqrt{N}}\sum_k e^{-i2\pi\omega kj}|k\rangle,$$

we can get a duality form of the Hamiltonian (1) with $\lambda_{l\geqslant 2} = 0$, given by

$$\tilde{H} = \sum_k (\lambda_L |k\rangle\langle k+1| + \lambda_R |k+1\rangle\langle k| + t_k |k\rangle\langle k|), \quad (38)$$

where $\lambda_L = \lambda_1 e^{-h}$, $\lambda_R = \lambda_1 e^h$, and $t_k = 2\cos(2\pi\omega k + ig)$. The Hamiltonian (1) with $\lambda_{l\geqslant 2} = 0$ and (38) have similar formulas, only with different coefficients, but they have the same spectrum, although the wave functions of the two Hamiltonians are entirely different. Let λ_1 denote the unit of energy. We can relabel $g' = h$, $h' = g$, $\lambda' = 1/\lambda_1$. Now we can see that the case of Fig. 8(a) with a fixed g and different h can be mapped to the case with a fixed h' and different g', i.e., the case of Fig. 8(b) in the dual Hamiltonian (38). So we can apply a similar explanation as to why the spectrum is invariant in the region of $g' < |g'_c|$ ($h < |h_c|$) for fixed h' (g). We note that under the dual transformation, the flux phase factor ψ is transformed to the phase factor ϕ', i.e., $H(\psi, \lambda_1, h, g)$ is mapping to $\tilde{H}(\phi', \lambda', h', g')$. Therefore, from the definitions of Eqs. (28) and (37), we find that $\nu_{\phi,\psi}$ can be related by the following relation:

$$\nu_\psi(\lambda_1, h, g) = \nu_\phi(1/\lambda_1, g, h), \quad (39)$$

i.e., ν_ψ for the system with parameters λ_1, h, and g can be obtained from ν_ϕ of the corresponding system with $\lambda' = 1/\lambda_1$, $h' = g$, and $g' = h$.

From the phase diagrams in Fig. 4, we always have $\nu_\phi = 0$ in the extended region and $\nu_\psi = \pm 1$. Nonzero winding number ν_ψ indicates the existence of skin states for the system under OBC [79–81]. On the other hand, we have always $\nu_\psi = 0$ in the localized region and $\nu_\phi = \pm 1$. The relation (39) constructs a mapping between the phase diagram of $\lambda_1 < 1$ and that of $\lambda_1 > 1$. The winding number ν_ϕ (ν_ψ) in Fig. 4(a) can be read out from ν_ψ (ν_ϕ) in Fig. 4(b) and vice versa.

By comparing the dual Hamiltonian (38) with the original Hamiltonian (1) with $\lambda_{l\geqslant 2} = 0$, we can see the existence of a self-duality point at $g = h$ and $\lambda_1 = 1$. At this self-duality point, $\lambda_c = 1$ is usually taken as the localization-delocalization transition point [59]. From Eq. (27), we have seen that $\lambda_c = 1$ is a transition point when $|h| = |g|$, i.e., the self-duality relation is only a special case of our general result Eq. (27). It is worth noting that our analytical result Eq. (27) does not rely on the self-duality relation or even the dual transformation.

Next we compare the spectra of the system under PBC and OBC to see the sensitivity of spectra to the change of boundary conditions. If the non-Hermitian skin effect exists, the system shall display remarkably different eigenspectra under PBC and OBC [78–82]. In Figs. 9(a)–9(c), we show the spectra in the complex space spanned by $\text{Re}(E)$ and $\text{Im}(E)$ for systems with $\lambda_1 = 0.5$, $h = 1.5$, and $g = -1, 0.5$, and 1, respectively, under both PBC and OBC. As shown in Fig. 9(b), in the localized region, the spectra under PBC and OBC are almost the same except for several isolated points corresponding to edge states. On the other hand, the spectra under PBC and OBC are obviously different in the delocalized region as shown in Figs. 9(a) and 9(c), which is a signature of the existence of the skin effect under OBC as witnessed in the distributions of eigenstates shown in Figs. 9(d) and
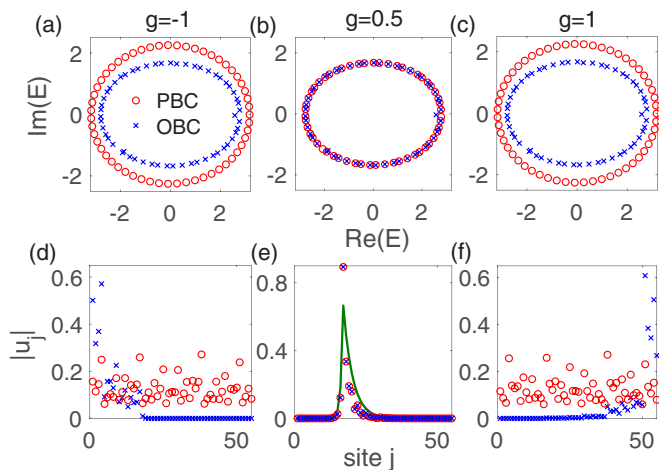
FIG. 9. (a)–(c) The complex spectrum for systems with $\lambda_1 = 0.5$, $h = 1.5$, $N = 55$, and $g = -1$, 0.5, and 1, respectively. The red circles and blue crosses represent the eigenvalues under PBC and OBC, respectively. (d)–(f) The distribution of eigenstates corresponding to the minimum real part of eigenvalues for systems with $\lambda_1 = 0.5$, $h = 1.5$, $g = -1$, 0.5, and 1, respectively. The solid line in (e) is plotted by using Eq. (24).

FIG. 10. (a) The real and the imaginary part of the eigenvalue spectra vs h for the system with potential (40). Here $g = 0$, $\lambda = 0.5$, $b = 0.1$, and $N = 55$. (b) The LE of eigenstates corresponding to the minimum (circles) and maximum (dots) real part of the eigenvalues. For accuracy of LE, we choose $N = 1597$. (c1) and (c2) The distribution of eigenstates corresponding to the minimum real part of eigenvalues for systems with $\lambda = 0.5$, $h = 1.2$, $g = 0.1$, and 0.8, respectively. (c3) and (c4) The distribution of eigenstates corresponding to the maximum real part of eigenvalues for systems with $\lambda = 0.5$, $h = 1.2$, $b = 0.1$, $g = 0.1$, and 0.8, respectively. The solid lines in (c1) and (c3) are plotted by using Eq. (24). In (c), $N = 55$.

9(f), respectively. The distributions of localized states under PBC and OBC are identical, as shown in Fig. 9(e), showing clearly that the localized states are independent of the boundary conditions. The numerical results also indicate that the distributions of localized states can be well described by Eq. (24).

V. APPLICATION TO OTHER MODELS

A. Generalized Ganeshan-Pixley–Das Sarma model

Next we consider the generalized complex Ganeshan-Pixley–Das Sarma model [22]

$$V_j = 2\lambda \frac{\cos(2\pi\omega j + ih)}{1 - b\cos(2\pi\omega j + ih)}, \quad (40)$$

which is the first quasiperiodic model in which the mobility edges have an analytic formula for the Hermitian case ($g, h = 0$). By applying Avila's global theory, the LE of the non-Hermitian model can be easily derived, and the expression is

$$\gamma(E, h) = \max\left\{|h| + \ln \frac{|bE + 2\lambda| + \sqrt{(bE+2\lambda)^2 - 4b^2}}{2(1+\sqrt{1-b^2})}, 0\right\}, \quad (41)$$

when $|h| < \ln|\frac{1+\sqrt{1-b^2}}{b}|$. The slope of $\gamma(E, h)$ might be ± 1 or 0. Figure 10(a) shows the spectrum for the system with $g = 0$, $\lambda = 0.5$, and $b = 0.1$ versus h. The spectrum does not change with h in the extended-state region: $h < 0.5$. This indicates clearly the existence of a robust spectrum in the complex Ganeshan-Pixley–Das Sarma model. For $h > 0.5$, the eigenstates with a high real part of energies become localized first, thus the LE of eigenstates corresponding to the minimum and maximum real part of eigenvalues can determine the mobility edge region, as shown in Fig. 10(b). In the region $h > 0.95$, all eigenstates are localized. Then we consider the system

with $g \neq 0$. The wave function (24) and the transition point (25) tell us that when $|g| < \gamma$, the states stay localized, while when $|g| > \gamma$, the states become extended, where γ is the LE with $g = 0$. Figure 10(c) shows the distribution of eigenstates corresponding to the minimum and maximum real part of the eigenvalues for systems with $h = 1.2$. Eigenstates are localized with $g = 0.1$ and are extended with $g = 0.8$, as shown in Fig. 10(c).

B. Quasiperiodic exponential potential

The nonreciprocal hopping model with the quasiperiodic exponential potential

$$V_j = V e^{i(2\pi\omega j + \phi)} \quad (42)$$

has the same basic idea to determine the transition point (25). The LE of the localized states for this model with $g = 0$ is $\gamma = \ln(V)$, so the boundary of the localization transition is given by

$$|V| = e^{|g|}. \quad (43)$$

The full details for the calculation of the LE are given in the Appendix A. While all eigenstates are localized for $|V| > e^{|g|}$, the eigenstates are extended states (skin states) under PBC (OBC) for $|V| < e^{|g|}$. When $g = 0$, the model reduces to the one studied in Ref. [54] and no skin effect occurs. For $g \neq 0$, the skin effect occurs in the region of $|V| < e^{|g|}$.

The unusual spectrum feature can also be found in this model. Equation (43) suggests that the localized phase exists only for $|V| > 1$. For a given V with $|V| > 1$, the system is in the localized phase in the region $|g| < g_c$ with $g_c = \ln|V|$. We find that the spectrum of the system is invariant with the change of g as long as $|g| < g_c$, which is verified by our numerical result and can be explained in a similar way to that presented in the above subsection.

VI. SUMMARY AND OUTLOOK

In summary, based on Avila's global theory, which was part of his Fields Medal work, we developed a rigorous and general scheme for the study of non-Hermitian quasiperiodic systems with both a complex phase factor and nonreciprocal hopping. We demonstrated that the localization-delocalization transition point, i.e., the $\mathcal{PT}$-symmetry-breaking point for general non-Hermitian quasicrystals with $h \neq 0$, can be described by a conclusive expression $h = \min\{\chi_1(E)\}$, where $\chi_1(E)$ is the smallest positive LE of its dual model with $h = 0$ for a given eigenvalue E. The general relation between winding numbers and acceleration is also unveiled. Consequently, we obtained that the winding number is just the slope of LE, and the topological transition points for the winding numbers are determined by all dual-model LEs $h = \chi_i(E)$. These results are applied to study the typical examples, including both the non-Hermitian AA model and the Soukoulis-Economou model. In particular, for the non-Hermitian AA model we analytically determined the complete phase diagram in the whole parameter space, which can be alternatively characterized by winding numbers. Moreover, we discovered an intriguing feature of the robust spectrum, i.e., the spectrum remains invariant under the change of the complex phase parameter h or nonreciprocal parameter g as long as $h < |h_c|$ or $g < |g_c|$ for the system in the extended or localized region, respectively. We found that the existence of the robust spectrum is a very common feature of non-Hermitian quasiperiodic systems. Models beyond the two typical examples are also discussed. Our analysis opens a door to further study of intriguing properties of non-Hermitian quasicrystals.

Photonic systems provide a valid platform of realization of non-Hermitian Hamiltonians with quasiperiodic potentials, which are manifested by the gain and loss of the laser pulse inside the optic fiber. Many typical phenomena have been observed in photonic experiments, such as $\mathcal{PT}$ symmetry, exceptional points, the non-Hermitian skin effect, etc. [83–88]. We expect that our theoretical work will stimulate an experimental study of the localization transition in non-Hermitian quasiperiodic systems.

APPENDIX A: GLOBAL THEORY OF THE ONE-FREQUENCY COCYCLE

Suppose that A is an analytic function from the circle S^1 to the group $SL(2, C)$. An analytic quasiperiodic cocycle (ω, A) can be seen as a linear skew product:

$$(\omega, A): S^1 \times R^2 \to S^1 \times R^2,$$
$$(\theta, v) \mapsto (\theta + \omega, A(\theta) \cdot v).$$

If $A(\theta)$ admits a holomorphic extension to $|\text{Im}\theta| < \delta$, then for $|\epsilon| < \delta$ we can define $A_\epsilon(\theta) = A(\theta + i\epsilon)$, and define its LE by

$$\gamma(E, h) = \lim_{n \to \infty} \frac{1}{2\pi n} \int_0^{2\pi} \ln ||T_n(E, \phi, h)|| d\phi, \quad \text{(A1)}$$

where T_n is the transfer matrix. The key observation of Avila's global theory is that $h \to \gamma(E, h)$ is convex and piecewise linear, with right-derivatives satisfying

$$\lim_{h \to 0_+} \frac{1}{2\pi h}[\gamma(E, h) - \gamma(E, 0)] \in \mathbb{Z}.$$

Similarly, the left-derivative satisfies

$$\lim_{h \to 0_-} \frac{1}{2\pi h}[\gamma(E, h) - \gamma(E, 0)] \in \mathbb{Z}.$$

Note that a sequence $(u_n)_{n \in \mathbb{Z}}$ is a formal solution of the eigenvalue equation

$$u_{n+1} + u_{n-1} + V(\theta + n\omega)u_n = Eu_n$$

if and only if it satisfied

$$\begin{pmatrix} u_{n+1} \\ u_n \end{pmatrix} = \begin{pmatrix} E - v(\theta + n\omega) & -1 \\ 1 & 0 \end{pmatrix} \begin{pmatrix} u_n \\ u_{n-1} \end{pmatrix},$$

therefore any quasiperiodic model (1) can be seen as a quasiperiodic cocycle.

Generally speaking, it is difficult to exactly calculate the LE, however Avila's global theory actually provides an efficient way to calculate the LE, and thus to determine the localize-delocalize transition. In the following, we will illustrate this by two well-known models, and we will explain the general results.

1. AA model

The eigenvalue equation of the AA model is

$$u_{n+1} + u_{n-1} + 2\lambda_1 \cos 2\pi(\theta + n\omega)u_n = Eu_n,$$

thus the corresponding cocycle is $(\omega, T(\theta))$, where

$$T(\theta) = \begin{pmatrix} E - 2\cos\theta & -1 \\ 1 & 0 \end{pmatrix}.$$

Let us complexify the phase, and let $h \to +\infty$. Direct computation shows that

$$T(\phi + ih) = e^h e^{i2\pi(\theta + \omega)} \begin{pmatrix} -\lambda & 0 \\ 0 & 0 \end{pmatrix} + o(1).$$

Thus we have $\gamma(E, h) = h + \log|\lambda| + o(1)$. Note $\gamma(E, h)$ is a convex, piecewise linear function of h with their slopes being integers, thus if h is large enough,

$$\gamma(E, h) = h + \log|\lambda|.$$

Furthermore, E does not lie in the spectrum of the Hamiltonian H if and only if $\gamma(E, h) > 0$, and $\gamma(E, h)$ is a linear function around h. Thus if the energy E lies in the spectrum, we have

$$\gamma(E, h) = \max\{\ln|\lambda| + h, 0\}, \ \forall h \geqslant 0.$$

Note that $T(\theta) \in SL(2, \mathbb{R})$, thus the LE is an even function with respect to h, which gives

$$\gamma(E, h) = \max\{\ln|\lambda| + |h|, 0\}, \ \forall h \in \mathbb{R}.$$

2. Complex quasiperiodic potential

For the complex quasiperiodic model $V_n = V e^{-i(2\pi\omega n + \phi)}$, the transfer matrix takes the form

$$T(\phi) = \begin{pmatrix} E - V e^{i(2\pi\omega + \phi)} & -1 \\ 1 & 0 \end{pmatrix},$$

thus $T(\phi) \in SL(2, \mathbb{C})$, i.e., it does not belong to $SL(2, \mathbb{R})$ anymore, thus compared to the AA model the LE is not an even function with respect to h. Still if we complexify the phase, and let $h \to +\infty$, direct computation shows that

$$T(\phi + ih) = e^h e^{-i2\pi(\phi+\omega)} \begin{pmatrix} -V & 0 \\ 0 & 0 \end{pmatrix} + o(1).$$

Thus we have $\gamma(E, h) = h + \log|V| + o(1), h \geqslant 0$. Note that $\gamma(E, h)$ is a convex, piecewise linear function of h with their slopes being integers. then if the energy belongs to the spectrum, then

$$\gamma(E, h) = \max\{\ln|\lambda| + h, 0\}, \ \forall \, h \geqslant 0,$$

consequently, we have

$$\gamma(E, 0) = \max\{\ln|V|, 0\}.$$

On the other hand, for the model $V_n = V e^{i(2\pi\omega n + \phi)}$ we can complexify the phase, and let $h \to -\infty$, which gives us $\gamma(E, h) = -h + \log|V| + o(1), h \leqslant 0$. Similarly, we have

$$\gamma(E, 0) = \max\{\ln|V|, 0\}. \tag{A2}$$

3. General models

As we mentioned above, one of the fundamental results of Avila's global theory is that $\gamma(E, h)$ is a piecewise affine function in h for each E, and the slope of each piece is an integer. Indeed, as proved in [71], one can give the exact turning points of $\gamma(E, h)$ and the exact slope of it in every piece, which can be seen as a quantitative version of Avila's global theory. In the following, we will try to explain this.

For any trigonometric polynomials

$$V_j = \sum_{k=1} 2\lambda_l \cos(2l\pi\omega j),$$

consider the quasiperiodic model

$$E u_j = u_{j+1} + u_{j-1} + V_j u_j, \ j \in \mathbb{Z}. \tag{A3}$$

Through the transformation

$$u_j = \sum_k e^{i2\pi\omega k j} \tilde{u}_k, \ k \in \mathbb{Z},$$

the dual model has the form

$$E\tilde{u}_k = \sum_{l=-d}^{d} \lambda_{|l|} \tilde{u}_{k+l} + 2\cos(2\pi\omega k)\tilde{u}_k. \tag{A4}$$

The model (A4) can be written as the following form:

$$\tilde{u}_{k+d} = \frac{1}{\lambda_d}\left\{[E - 2\cos(2\pi\omega k)]\tilde{u}_k - \sum_{l=-d}^{d-1} \lambda_{|l|}\tilde{u}_{k+l}\right\}. \tag{A5}$$

So the matrix form for the model (A5) can be written as

$$\begin{pmatrix} \tilde{u}_{k+d} \\ \vdots \\ \tilde{u}_{k+1} \\ \tilde{u}_k \\ \vdots \\ \tilde{u}_{k-d+1} \end{pmatrix} = A^k \begin{pmatrix} \tilde{u}_{k+d-1} \\ \vdots \\ \tilde{u}_k \\ \tilde{u}_{k-1} \\ \vdots \\ \tilde{u}_{k-d} \end{pmatrix},$$

where

$$A^k = \begin{pmatrix} \frac{-\lambda_{d-1}}{\lambda_d} & \cdots & \frac{E-2\cos(2\pi\omega k)}{\lambda_d} & \frac{-\lambda_1}{\lambda_d} & \cdots & -1 \\ 1 & \cdots & 0 & 0 & \cdots & 0 \\ 0 & \ddots & & & & 0 \\ \vdots & & 1 & & & \vdots \\ & & & & \ddots & \\ 0 & \cdots & & & 1 & 0 \end{pmatrix}$$

is a $2d \times 2d$ matrix. Then we can define the matrix

$$\Theta = \left(T_N^\dagger T_N\right)^{1/(2N)}, \tag{A6}$$

where $T_N = \prod_k A^k$ is the total transfer matrix. When $N \to \infty$, Θ is finite, which can be guaranteed by Oseledec's ergodic theorem. The LEs are

$$\chi_i = \ln\theta_i,$$

where θ_i are the eigenvalues of matrix Θ.

It is easy to check that

$$T^{dn} = \prod_{k=dn}^{dn+d-1} A^k = \begin{pmatrix} C_d^{-1}(EI - B_{dn}) & -C_d^{-1}C_d^* \\ I_d & O_d \end{pmatrix}, \tag{A7}$$

where

$$C_d = \begin{pmatrix} \lambda_d & \cdots & \lambda_1 \\ 0 & \ddots & \vdots \\ 0 & 0 & \lambda_d \end{pmatrix},$$

C_d^* is its adjoint, and B_{dn} is the Hermitian matrix,

$$B_{dn} = \begin{pmatrix} W_{dn+n-1} & \lambda_1 & \cdots & \lambda_{d-1} \\ \lambda_1 & \ddots & \ddots & \vdots \\ \vdots & \ddots & W_{dn+1} & \lambda_1 \\ \lambda_{d-1} & \cdots & \lambda_1 & W_{dn} \end{pmatrix},$$

where $W_k = 2\cos(2\pi\omega k)$, and I_d and O_d are the d-dimensional identity and zero matrices.

Note that the matrix (A7) is complex symplectic, thus the eigenvalues of (A6) will come in pairs. The LEs can then be denoted by $\pm\chi_1, \ldots, \pm\chi_\ell$ with multiplicity $n_1, \ldots, n_\ell$, respectively. We may assume that $0 \leqslant \chi_1(E) < \cdots < \chi_\ell(E)$. It is obvious that $n_1 + \cdots + n_\ell = d$.

As proved in [71], the LEs for the model (1) with $g = 0$ can be written as the following:

$$\gamma(E, h) = \begin{cases} \gamma(E, 0), & h \in [0, \chi_1(E)], \\ \quad\vdots & \quad\vdots \\ \gamma(E, \chi_i(E)) + [h - \chi_i(E)] \sum_{j=1}^{i} n_j, & h \in (\chi_i(E), \chi_{i+1}(E)], \\ \quad\vdots & \quad\vdots \\ \gamma(E, \chi_\ell(E)) + [h - \chi_l(E)] \sum_{j=1}^{\ell} n_j, & h \in (\chi_\ell(E), \infty), \end{cases} \tag{A8}$$

where $E \in \mathbb{C}$ and $1 < i < \ell$. For the $\mathcal{PT}$-symmetrical case, the model (1) with $g = 0$, the boundaries of the extended-mixed transformation and mixed-localized transformation can be determined by $h = \min(\chi_1(E))$ and $h = \max(\chi_1(E))$, which only depends on $\chi_1(E)$ in connection with longest localization length for the dual model (A5).

APPENDIX B: WINDING NUMBER ν_ϕ FOR $g = 0$ AND $g \neq 0$

The definition of winding number ν_ϕ is

$$\nu_\phi(g) = \lim_{N \to \infty} \frac{1}{2\pi i} \int_0^{2\pi} d\phi \, \partial_\phi \frac{\ln \det[H(\theta, g) - E_B]}{N}$$

$$= \lim_{N \to \infty} \frac{1}{2\pi i} \int_0^{2\pi} d\phi \, \partial_\phi \zeta(E_B, \theta, g), \tag{B1}$$

where $\theta = \phi + ih$ and the analytical function

$$\zeta(E_B, \theta, g) = \frac{\ln D_n(E_B, \theta, g)}{N} \tag{B2}$$

with

$$D_n(E_B, \theta, g) = \det|H(\theta, g) - E_B|.$$

According to the Cauchy-Riemann equation in complex form, we can get

$$\frac{\partial \zeta(E_B, \theta, g)}{\partial h} = i \frac{\partial \zeta(E_B, \theta, g)}{\partial \phi}. \tag{B3}$$

Then we can get

$$\nu_\phi = \frac{1}{2\pi i} \lim_{N \to \infty} \int_0^{2\pi} d\phi \, \partial_\phi \zeta(E_B, \theta, g)$$

$$= -\frac{1}{2\pi} \lim_{N \to \infty} \int_0^{2\pi} d\phi \, \partial_h \zeta(E_B, \theta, g)$$

$$= -\frac{1}{2\pi} \lim_{N \to \infty} \partial_h \int_0^{2\pi} d\phi \, \zeta(E_B, \theta, g).$$

When $g = 0$ and $n \to \infty$, the normal of the transfer matrix is

$$\lim_{n \to \infty} \frac{\ln \|T_n(E_B, \theta)\|}{N} = \lim_{n \to \infty} \zeta(E_B, \theta, 0).$$

The transfer matrix of the system with $g = 0$ can be written as

$$T_n(E, \theta) = \prod_{j=1}^{n} T^j = \prod_{j=1}^{n} \begin{pmatrix} E - V_j & -1 \\ 1 & 0 \end{pmatrix}.$$

The transfer matrix can also be expressed as

$$T_n(E, \theta) = \begin{pmatrix} D_n(E_B, \theta, 0) & -D_{n-1}(E_B, \theta, 0) \\ D_{n-1}(E_B, \theta, 0) & -D_{n-2}(E_B, \theta, 0). \end{pmatrix}$$

Then we can get

$$\lim_{N \to \infty} \int_0^{2\pi} d\phi \, \zeta(E_B, \theta, 0)$$

$$= \lim_{N \to \infty} \int_0^{2\pi} d\phi \, \frac{\ln \|T_N(E_B, \theta)\|}{N}$$

$$= 2\pi \gamma(E_B, h).$$

Finally, we get the relation

$$\nu_\phi(0) = -\partial_h \gamma(E_B, h).$$

Now, we calculate the winding number of system with $g \neq 0$. The Hamiltonian with a general boundary condition in matrix form can be written as

$$H(\phi, g) = \begin{pmatrix} V_1 & 1 & & & \eta e^{Ng} \\ 1 & V_2 & 1 & & \\ & \ddots & \ddots & \ddots & \\ & & 1 & V_{N-1} & 1 \\ \eta e^{-Ng} & & & 1 & V_N \end{pmatrix}, \tag{B4}$$

where η is a finite value. $\eta = 0$ or 1 corresponds to PBC or OBC. In the large-N limit, the determinant of $H(\phi)$ is

$$\det H(\phi, g) = (-1)^{N+1} \eta e^{N|g|} - 2 \times (-1)^{N+1} + \det H(\phi, 0).$$

First we calculate the integrand

$$\frac{1}{2\pi i} \partial_\phi \frac{\ln[D(E_B, \theta, g)]}{N}$$

$$= \frac{1}{2\pi i} \frac{\partial_\phi D(E_B, \theta, 0)}{N D(E_B, \theta, g)}$$

$$= \frac{1}{2\pi i} \frac{\partial_\phi D(E_B, \theta, 0)}{N[(-1)^{N+1} \eta e^{Ng} + D(E_B, \theta, 0)]}.$$

To calculate the above equation, we need to get the behavior of $\partial_\phi D(E_B, \theta, 0)$ and $D(E_B, \theta, 0)$. According to the definition of the LE,

$$\lim_{N \to \infty} \ln|D(E_B, \theta, 0)|/N = \gamma \tag{B5}$$

and thus $|D(E_B, \theta, 0)|$ can be written as

$$|D(E_B, \theta, 0)| = e^{\gamma N}.$$

According to the definition of the winding number,

$$\lim_{N \to \infty} \frac{1}{2\pi i} \int_0^{2\pi} d\phi \, \partial_\phi \frac{\ln \det[H(\theta, 0) - E_B]}{N} = \nu_\phi(0),$$

we can obtain

$$\frac{\partial_\phi D(E_B, \theta, 0)}{D(E_B, \theta, 0)} = N\Omega(\psi),$$

with

$$\lim_{N \to \infty} \int_0^{2\pi} \Omega(\psi) = 2\pi \nu_\phi(0) i.$$

Then, we can obtain

$$\frac{1}{2\pi i} \partial_\phi \frac{\ln[D(E_B, \theta, g)]}{N} = \begin{cases} 0, & |g| > \gamma, \\ \Omega(\psi), & |g| < \gamma \end{cases} \quad (B6)$$

for $\eta \neq 0$ and

$$\frac{1}{2\pi i} \partial_\phi \frac{\ln[D(E_B, \theta, g)]}{N} = \Omega(\psi) \quad (B7)$$

for $\eta = 0$. Finally, substitution of Eq. (B6) into Eq. (B1) yields the winding number of the system with $g \neq 0$ and $\eta \neq 0$,

$$\nu_\phi(g) = \lim_{N \to \infty} \frac{1}{2\pi i} \int_0^{2\pi} d\phi \, \partial_\phi \frac{\ln \det[H(\theta, g) - E_B]}{N}$$

$$= \begin{cases} 0, & |g| > \gamma, \\ \nu_\phi(0) = -\partial_h \gamma(E_B, h), & |g| < \gamma. \end{cases} \quad (B8)$$

Substitution of Eq. (B7) into Eq. (B1) yields the winding number of the system under OBC ($\eta = 0$),

$$\nu_\phi(g) = \nu_\phi(0). \quad (B9)$$

Thus we can see that the winding number remains unchanged under different boundary conditions except OBC.

[1] P. W. Anderson, Absence of diffusion in certain random lattices, Phys. Rev. **109**, 1492 (1958).

[2] E. Abrahams, P. W. Anderson, D. C. Licciardello, and T. V. Ramakrishnan, Scaling Theory of Localization: Absence of Quantum Diffusion in Two Dimensions, Phys. Rev. Lett. **42**, 673 (1979).

[3] D. J. Thouless, A relation between the density of states and range of localization for one dimensional random systems, J. Phys. C **5**, 77 (1972).

[4] P. A. Lee and T. V. Ramakrishnan, Disordered electronic systems, Rev. Mod. Phys. **57**, 287 (1985).

[5] F. Evers and A. D. Mirlin, Anderson transitions, Rev. Mod. Phys. **80**, 1355 (2008).

[6] G. Roati, C. DErrico, L. Fallani, M. Fattori, C. Fort, M. Zaccanti, G. Modugno, M. Modugno, and M. Inguscio, Anderson localization of a non-interacting bose einstein condensate, Nature (London) **453**, 895 (2008).

[7] H. P. Lüschen, S. Scherg, T. Kohlert, M. Schreiber, P. Bordia, X. Li, S. Das Sarma, and I. Bloch, Single-Particle Mobility Edge in a One-Dimensional Quasiperiodic Optical Lattice, Phys. Rev. Lett. **120**, 160404 (2018).

[8] S. Aubry and G. André, Analyticity breaking and Anderson localization in incommensurate lattices, Ann. Isr. Phys. Soc. **3**, 133 (1980).

[9] D. J. Thouless, Localization by a Potential with Slowly Varying Period, Phys. Rev. Lett. **61**, 2141 (1988).

[10] M. Kohmoto, Metal-Insulator Transition and Scaling for Incommensurate Systems, Phys. Rev. Lett. **51**, 1198 (1983).

[11] S. Y. Jitomirskaya, Metal-insulator transition for the almost mathieu operator, Ann. Math. **150**, 1159 (1999).

[12] H. A. Ceccatto, Quasiperiodic Ising Model in a Transverse Field: Analytical Results, Phys. Rev. Lett. **62**, 203 (1989).

[13] L. Zhou, H. Pu, and W. Zhang, Anderson localization of cold atomic gases with effective spin-orbit interaction in a quasiperiodic optical lattice, Phys. Rev. A **87**, 023625 (2013).

[14] M. Kohmoto and D. Tobe, Localization problem in a quasiperiodic system with spin-orbit interaction, Phys. Rev. B **77**, 134204 (2008).

[15] X. Cai, L.-J. Lang, S. Chen, and Y. Wang, Topological Superconductor to Anderson Localization Transition in One-Dimensional Incommensurate Lattices, Phys. Rev. Lett. **110**, 176403 (2013).

[16] W. DeGottardi, D. Sen, and S. Vishveshwara, Majorana Fermions in Superconducting 1D Systems Having Periodic, Quasiperiodic, and Disordered Potentials, Phys. Rev. Lett. **110**, 146404 (2013).

[17] F. Liu, S. Ghosh, and Y. D. Chong, Localization and adiabatic pumping in a generalized Aubry-Andre-Harper model, Phys. Rev. B **91**, 014108 (2015).

[18] A. Chandran and C. R. Laumann, Localization and Symmetry Breaking in the Quantum Quasiperiodic Ising Glass, Phys. Rev. X **7**, 031061 (2017).

[19] Y.-C. Wang, X.-J. Liu, and S. Chen, Properties and applications of one dimensional quasiperiodic lattices, Acta Phys. Sin. **68**, 040301 (2019).

[20] J. Biddle, D. J. Priour, B. Wang, and S. Das Sarma, Localization in one-dimensional lattices with non-nearest-neighbor hopping: Generalized Anderson and Aubry-André models, Phys. Rev. B **83**, 075105 (2011).

[21] J. Biddle and S. Das Sarma, Predicted Mobility Edges in One-Dimensional Incommensurate Optical Lattices: An Exactly Solvable Model of Anderson Localization, Phys. Rev. Lett. **104**, 070601 (2010).

[22] S. Ganeshan, J. H. Pixley, and S. Das Sarma, Nearest Neighbor Tight Binding Models with an Exact Mobility Edge in One Dimension, Phys. Rev. Lett. **114**, 146601 (2015).

[23] X. P. Li, J. H. Pixley, D. L. Deng, S. Ganeshan, and S. Das Sarma, Quantum nonergodicity and fermion localization in a system with a single-particle mobility edge, Phys. Rev. B **93**, 184204 (2016).

[24] X. Li, X. P. Li, and S. Das Sarma, Mobility edges in one-dimensional bichromatic incommensurate potentials, Phys. Rev. B **96**, 085119 (2017).

[25] X. Li and S. Das Sarma, Mobility edge and intermediate phase in one-dimensional incommensurate lattice potentials, Phys. Rev. B **101**, 064203 (2020).

[26] X. Deng, S. Ray, S. Sinha, G. V. Shlyapnikov, and L. Santos, One-Dimensional Quasicrystals with Power-Law Hopping, Phys. Rev. Lett. **123**, 025301 (2019).

[27] S. Das Sarma, S. He, and X. C. Xie, Mobility Edge in a Model One-Dimensional Potential, Phys. Rev. Lett. **61**, 2144 (1988).

[28] S. Das Sarma, S. He, and X. C. Xie, Localization, mobility edges, and metal-insulator transition in a class of

one-dimensional slowly varying deterministic potentials, Phys. Rev. B **41**, 5544 (1990).

[29] Y. Wang, X. Xia, L. Zhang, H. Yao, S. Chen, J. You, Q. Zhou, and X. Liu, One Dimensional Quasiperiodic Mosaic Lattice with Exact Mobility Edges, Phys. Rev. Lett. **125**, 196604 (2020).

[30] D. Bernard and A. LeClair, A classification of non-Hermitian random matrices, in *Statistical Field Theories*, edited by A. Cappelli and G. Mussardo, NATO Science Series (Series II: Mathematics, Physics and Chemistry) (Springer, Dordrecht, 2002), Vol. 73.

[31] K. Kawabata, K. Shiozaki, M. Ueda, and M. Sato, Symmetry and Topology in Non-Hermitian Physics, Phys. Rev. X **9**, 041015 (2019).

[32] H. Zhou and J. Y. Lee, Periodic table for topological bands with non-Hermitian symmetries, Phys. Rev. B **99**, 235112 (2019).

[33] C.-H. Liu and S. Chen, Topological classification of defects in non-Hermitian systems, Phys. Rev. B **100**, 144106 (2019).

[34] I. Y. Goldsheid and B. A. Khoruzhenko, Distribution of Eigenvalues in Non-Hermitian Anderson Models, Phys. Rev. Lett. **80**, 2897 (1998).

[35] L. G. Molinari, Non-Hermitian spectra and Anderson localization, J. Phys. A **42**, 265204 (2009).

[36] H. Markum, R. Pullirsch, and T. Wettig, Non-Hermitian Random Matrix Theory and Lattice QCD with Chemical Potential, Phys. Rev. Lett. **83**, 484 (1999).

[37] J. T. Chalker and B. Mehlig, Eigenvector Statistics in Non-Hermitian Random Matrix Ensembles, Phys. Rev. Lett. **81**, 3367 (1998).

[38] R. Hamazaki, K. Kawabata, N. Kura, and M. Ueda, Universality classes of non-hermitian random matrices, Phys. Rev. Res. **2**, 023286 (2020).

[39] C. Wang and X. R. Wang, Level statistics of extended states in random non-Hermitian Hamiltonians, Phys. Rev. B **101**, 165114 (2020).

[40] X. Luo, T. Ohtsuki, and R. Shindou, Universality Classes of the Anderson Transitions Driven by Non-Hermitian Disorder, Phys. Rev. Lett. **126**, 090402 (2021).

[41] K. Kawabata and S. Ryu, Nonunitary Scaling Theory of Non-Hermitian Localization, Phys. Rev. Lett. **126**, 166801 (2021).

[42] N. Hatano and D. R. Nelson, Localization Transitions in Non-Hermitian Quantum Mechanics, Phys. Rev. Lett. **77**, 570 (1996).

[43] N. Hatano and D. R. Nelson, Non-Hermitian delocalization and eigenfunctions, Phys. Rev. B **58**, 8384 (1998).

[44] A. V. Kolesnikov and K. B. Efetov, Localization-Delocalization Transition in Non-Hermitian Disordered Systems, Phys. Rev. Lett. **84**, 5600 (2000).

[45] Z. Gong, Y. Ashida, K. Kawabata, K. Takasan, S. Higashikawa, and M. Ueda, Topological Phases of Non-Hermitian Systems, Phys. Rev. X **8**, 031079 (2018).

[46] D.-W. Zhang, L.-Z. Tang, L.-J. Lang, H. Yan, and S.-L. Zhu, Non-hermitian topological anderson insulators, Sci. China Phys. Mech. **63**, 267062 (2020).

[47] J. Claes and T. L. Hughes, Skin effect and winding number in disordered non-Hermitian systems, Phys. Rev. B **103**, L140201 (2021).

[48] L.-Z. Tang, L.-F. Zhang, G.-Q. Zhang, and D.-W. Zhang, Topological Anderson insulators in two-dimensional non-Hermitian disordered systems, Phys. Rev. A **101**, 063612 (2020).

[49] Y. Huang and B. I. Shklovskii, Anderson transition in three-dimensional systems with non-Hermitian disorder, Phys. Rev. B **101**, 014204 (2020).

[50] A. F. Tzortzakakis, K. G. Makris, and E. N. Economou, Non-Hermitian disorder in two-dimensional optical lattices, Phys. Rev. B **101**, 014202 (2020).

[51] A. Jazaeri and I. I. Satija, Localization transition in incommensurate non-Hermitian systems, Phys. Rev. E **63**, 036222 (2001).

[52] C. Yuce, $\mathcal{PT}$ symmetric Aubry-Andre model, Phys. Lett. A **378**, 2024 (2014).

[53] Q.-B. Zeng, S. Chen, and R. Lu, Anderson localization in the non-Hermitian Aubry-Andre-Harper model with physical gain and loss, Phys. Rev. A **95**, 062118 (2017).

[54] S. Longhi, Metal-insulator phase transition in a non-Hermitian Aubry-André-Harper model, Phys. Rev. B **100**, 125157 (2019).

[55] S. Longhi, Topological Phase Transition in Non-Hermitian Quasicrystals, Phys. Rev. Lett. **122**, 237601 (2019).

[56] H. Jiang, L. J. Lang, C. Yang., S. L. Zhu, and S. Chen, Interplay of non-Hermitian skin effects and Anderson localization in nonreciprocal quasiperiodic lattices, Phys. Rev. B **100**, 054301 (2019).

[57] Q. B. Zeng, Y. B. Yang, and Y. Xu, Topological phases in non-Hermitian Aubry-André-Harper models, Phys. Rev. B **101**, 020201(R) (2020).

[58] Y. Liu, X.-P. Jiang, J. Cao, and S. Chen, Non-Hermitian mobility edges in one-dimensional quasicrystals with parity-time symmetry, Phys. Rev. B **101**, 174205 (2020).

[59] Q.-B. Zeng and Y. Xu, Winding numbers and generalized mobility edges in non-Hermitian systems, Phys. Rev. Res. **2**, 033052 (2020).

[60] T. Liu, H. Guo, Y. Pu, and S. Longhi, Generalized Aubry-Andre self-duality and mobility edges in non-Hermitian quasiperiodic lattices, Phys. Rev. B **102**, 024205 (2020).

[61] Y. Liu, Y. Wang, X.-J. Liu, Q. Zhou, and S. Chen, Exact mobility edges, PT-symmetry breaking and skin effect in one-dimensional non-Hermitian quasicrystals, Phys. Rev. B **103**, 014203 (2021).

[62] X. Cai, Boundary-dependent self-dualities, winding numbers and asymmetrical localization in non-Hermitian quasicrystals, Phys. Rev. B **103**, 014201 (2021).

[63] S. Longhi, Phase transitions in a non-Hermitian Aubry-André-Harper model, Phys. Rev. B **103**, 054203 (2021).

[64] L.-J. Zhai, S. Yin, and G.-Y. Huang, Many-body localization in a non-Hermitian quasi-periodic system, Phys. Rev. B **102**, 064206 (2020).

[65] Y. Liu, Y. Wang, Z. Zheng, and S. Chen, Exact non-Hermitian mobility edges in one-dimensional quasicrystal lattice with exponentially decaying hopping and its dual lattice, Phys. Rev. B **103**, 134208 (2021).

[66] L.-Z. Tang, G.-Q. Zhang, L.-F. Zhang, and D.-W. Zhang, Localization and topological transitions in non-Hermitian quasiperiodic lattices, Phys. Rev. A **103**, 033325 (2021).

[67] X. Cai, Anderson localization and topological phase transitions in non-Hermitian Aubry-André-Harper models with p-wave pairing, Phys. Rev. B **103**, 214202 (2021).

[68] A. Avila, Global theory of one-frequency Schrödinger operators, Acta. Math. **215**, 1 (2015).

[69] A. Avila, J. You, and Q. Zhou, Sharp phase transitions for the almost Mathieu operator, Duke. Math. J. **166**, 2697 (2017).

[70] C. M. Bender and S. Boettcher, Real Spectra in Non-Hermitian Hamiltonians Having PT Symmetry, Phys. Rev. Lett. **80**, 5243 (1998).

[71] L. Ge, S. Y. Jitomirskaya, J. You, and Q. Zhou, Quantitative global theory of one-frequency quasiperiodic operators (unpublished).

[72] A. Avila and S. Y. Jitomirskaya, The ten martini problem, Ann. Math. **170**, 303 (2009).

[73] C. M. Soukoulis and E. N. Economou, Localization in One-Dimensional Lattices in the Presence of Incommensurate Potentials, Phys. Rev. Lett. **48**, 1043 (1982).

[74] S. Yao and Z. Wang, Edge States and Topological Invariants of Non-Hermitian Systems, Phys. Rev. Lett. **121**, 086803 (2018).

[75] Y. Xiong, Why does bulk boundary correspondence fail in some non-Hermitian topological models, J. Phys. Commun. **2**, 035043 (2018).

[76] V. M. Martinez Alvarez, J. E. Barrios Vargas, and L. E. F. Foa Torres, Non-Hermitian robust edge states in one dimension: Anomalous localization and eigenspace condensation at exceptional points, Phys. Rev. B **97**, 121401(R) (2018).

[77] F. K. Kunst, E. Edvardsson, J. C. Budich, and E. J. Bergholtz, Biorthogonal, Bulk-Boundary Correspondence in Non-Hermitian Systems, Phys. Rev. Lett. **121**, 026808 (2018).

[78] C. H. Lee and R. Thomale, Anatomy of skin modes and topology in non-Hermitian systems, Phys. Rev. B **99**, 201103(R) (2019).

[79] K. Yokomizo and S. Murakami, Non-Bloch Band theory of Non-Hermitian System, Phys. Rev. Lett. **123**, 066404 (2019).

[80] K. Zhang, Z. Yang, and C. Fang, Correspondence Between Winding Numbers and Skin Modes in Non-Hermitian Systems, Phys. Rev. Lett. **125**, 126402 (2020).

[81] N. Okuma, K. Kawabata, K. Shiozaki, and M. Sato, Topological Origin of Non-Hermitian Skin Effects, Phys. Rev. Lett. **124**, 086801 (2020).

[82] D. S. Borgnia, A. J. Kruchkov, and R.-J. Slager, Non-Hermitian Boundary Modes, Phys. Rev. Lett. **124**, 056802 (2020).

[83] A. Regensburger, C. Bersch, B. Hinrichs, G. Onishchukov, A. Schreiber, C. Silberhorn, and U. Peschel, Photon Propagation in a Discrete Fiber Network: An Interplay of Coherence and Losses, Phys. Rev. Lett. **107**, 233902 (2011).

[84] A. Regensburger, C. Bersch, M. A. Miri, G. Onishchukov, D. N. Christodoulides, and U. Peschel, Parity-time synthetic photonic lattices, Nature (London) **488**, 167 (2012).

[85] M. Wimmer, M. A. Miri, D. Christodoulides, and U. Peschel, Observation of Bloch oscillations in complex PT-symmetric photonic lattices, Sci. Rep. **5**, 17760 (2015).

[86] I. D. Vatnik, A. Tikan, G. Onishchukov, D. V. Churkin, and A. A. Sukhorukov, Anderson localization in synthetic photonic lattices, Sci. Rep. **7**, 4301 (2017).

[87] S. Derevyanko, Disorder-aided pulse stabilization in dissipative synthetic photonic lattices, Sci. Rep. **9**, 12883 (2019).

[88] S. Weidemann, M. Kremer, T. Helbig, T. Hofmann, A. Stegmaier, M. Greiter, R. Thomale, and A. Szameit, Topological funneling of light, Science **368**, 311 (2020).